Optimization of an Injection-Controlled Excimer Laser Guided by Analytical Modeling

C. Brent Dane, Thomas Hofmann, Roland Sauerbrey, *Senior Member, IEEE,* and Frank K. Tittel, *Fellow, IEEE*

Abstract—**The application of an analytical model describing the injection control of pulsed laser systems is successfully demonstrated for the design of a scaled XeF($C \rightarrow A$) excimer laser system. Enhancements to an earlier version of the model are described which improve the treatment of spatial beam overlap and saturation, unpumped volume, intracavity losses, and a noninteger number of round-trips in the unstable resonator. These result in the accurate simulation of injection-controlled laser performance over a wide range of unstable resonator magnifications, mirror spacings, and intracavity optical losses. Excellent agreement between calculated and experimentally observed energies and temporal profiles of the injection-controlled laser output was obtained.**

I. Introduction

THE injection control of laser systems has been used to successfully control the wavelength, bandwidth, and beam quality of a wide variety of lasers operating in the infrared [1]-[3], visible [4], [5], and ultraviolet [6]. Using a properly designed resonator, injection control is achievable with a very low input intensity threshold and high energy extraction efficiency. For a laser using an unstable resonator, the optimum design requires the choice of a cavity magnification which is correctly matched to the laser system. The most significant factors affecting this choice are the peak value and temporal duration of the small signal gain. However, careful consideration should also be given in the cavity design to factors such as the saturation dynamics of both gain and absorption, the length of unpumped beam path within the resonator, and round-trip losses, particularly in the case of a low gain laser medium.

For injection-controlled excimer lasers, it has been suggested that the optimum resonator magnification M can be estimated from the known optimum stable resonator output coupling $(1 - 1/M^2)$, with a small correction for the effects of diffraction from the edges of the output coupler [6]. This, however, is not feasible for laser systems which do not operate efficiently as a free-running oscillator, without injection control, and for which an optimum output coupling is therefore not known with certainty. Such is the case for the XeF($C \rightarrow A$) excimer laser used in this paper. It has been shown that relatively uncomplicated analytical models based on rate equation formulations can be used to accurately describe the injection control of excimer lasers [7]-[11]. One of these models, which is particularly adapted to the treatment of saturable absorption was successfully applied to a small scale XeF($C \rightarrow A$) laser operating in the blue-green [12].

Recently, a predictive tool was required to investigate the scaling of XeF($C \rightarrow A$) laser performance to large gain volumes and high output energies and this model was used successfully for this purpose [13]. This paper presents an expanded version of the previous analytical model as applied to a scaled XeF($C \rightarrow A$) laser. Enhancements were made to better describe spatial beam overlap and saturation, unpumped volume, intracavity losses, a noninteger number of round-trips in the unstable resonator, and off-axis resonator configurations. The results of numerical modeling and experimental measurements of the scaled XeF($C \rightarrow A$) injection-controlled laser are presented over a range of resonator magnifications, mirror spacings, and injection intensities.

II. The XeF($C \rightarrow A$) Laser System

The XeF($C \rightarrow A$) laser is an excimer laser system which is broadly tunable over the blue-green region of the spectrum. Using injection control, efficient, narrowband operation has been demonstrated between 450 and 530 nm [5]. Single pulse energies of over 0.8 J in 10 ns FWHM at 486.8 nm have been reported from a scaled electron-beam pumped XeF($C \rightarrow A$) laser with an active volume of ~0.5 L, corresponding to an energy density of 1.7 J/L and an intrinsic efficiency of 1.3% [14]. Using large aperture optics to increase the active volume to ~1 L, repetitive 1 Hz operation of this laser has recently been demonstrated with output energies of 1.2 J/pulse [15].

The XeF($C \rightarrow A$) electronic transition is characterized by a relatively long radiative lifetime, $\tau_{CA} \sim 100$ ns, and a small cross section for stimulated emission, $\sigma_{SE} \sim 1 \times 10^{-17}$ cm^2, as compared to $\tau_{BX} \sim 15$ ns and $\sigma_{SE} \sim 3.5 \times 10^{-16}$ cm^2 for the 353 nm ultraviolet XeF($B \rightarrow X$) transition. The latter values are also typical for other rare gas halide UV transitions. This is of significant consequence for the injection control of these excimer laser systems. For the comparably high gain UV lasers, the most important aspect of the injection process is the spectral and beam quality control of the laser output [6]. The laser can be

Manuscript received December 17, 1990; revised June 14, 1991.

The authors are with the Department of Electrical and Computer Engineering, Rice University, Houston, TX 77251.

IEEE Log Number 9103217.

tuned across the transition bandwidth with an output linewidth and wavelength controlled by the injection pulse. However, in a typical electron-beam pumped gas mixture, the XeF(C) state has an effective lifetime of only ~ 15 ns due to reactive quenching. For this reason, given the slow rate of spontaneous emission characterized by $\tau_{CA} = 100$ ns, the XeF($C \rightarrow A$) laser does not operate efficiently as a free-running oscillator when excited by a short, intense electron-beam pumping pulse. By supplying an injected optical field at the onset of gain, however, laser oscillation is not required to build up from spontaneous noise photons. Therefore, in the case of the XeF($C \rightarrow A$) laser, injection-control not only provides wavelength, linewidth, and beam quality control, but also results in the most efficient energy extraction from the gain medium.

A second consequence of the relatively small σ_{SE} for the XeF($C \rightarrow A$) transition is that the saturation intensity for the XeF($C \rightarrow A$) transition is higher than that of the primary transient absorbers. For this reason, the performance of this laser system depends critically on the saturation behavior of gain as well as that of absorption in the active medium. A model describing laser action in this system must therefore specifically treat the saturation of both the gain and the absorption. This, of course, results in a general formulation that continues to be applicable to other pulsed gas laser systems in which the background absorbers may not significantly saturate.

III. The Injection-Control Model

A. General Description

An analytical model has been developed to simulate the injection-control process in pulsed lasers as reported in [7]. There is a set of significant assumptions made in the formulation of the model under which its application is valid. Since no attempt is made to control the temporal phase of the injection pulse, as is the case when the *injection locking* technique is employed, a rate equation approach is used in which the laser is treated as a folded amplifier which is seeded by the injection beam. It is assumed that the laser transition is homogeneously broadened and that the injection bandwidth is significantly smaller than the tuning range of the laser transition, making possible a wavelength independent set of rate equations. The laser flux used in the calculations is the spectrally integrated photon flux which corresponds to the experimentally observable laser output intensity.

A one-dimensional computation is implemented by unfolding the laser amplifier and considering a single ray path through the resonator as shown in Fig. 1. A geometric optical analysis is used to treat light propagation in the unstable resonator and to estimate output coupling losses. This is a reasonable physical description for large Fresnel number resonators, such as those used in this study (Table I), in which the diffractive contributions to the round-trip cavity losses are small [16].

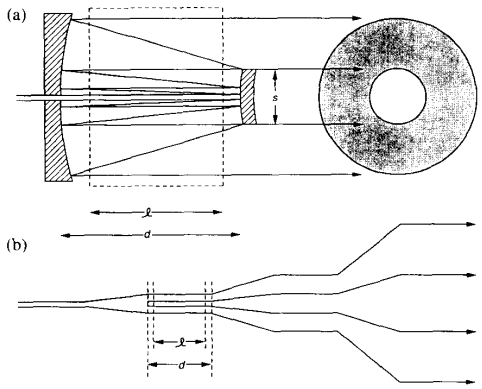

Fig. 1. (a) Schematic representation of an injection-controlled unstable resonator. l is the length of the laser gain medium and d is the resonator mirror spacing. The unstable cavity magnification is defined as the ratio of the outer diameter of the output beam to the diameter of the output coupler. (b) In order to describe the injection-control process with a one-dimensional model, the resonator is treated as a single-pass unfolded amplifier with corrections for overlapping beam passes.

TABLE I
A Summary of the Characteristics of the Four Unstable Resonators Used in This Study. M is the Resonator Magnification, d is the Mirror Spacing, l is the Length of the Gain Medium (50 cm), R_1 is the Radius of Curvature of the Concave Input Coupler, R_2 is the Radius of Curvature of the Convex Output Coupler, s is the Diameter of the Output Coupler, and N_{eq} is the Equivalent Fresnel Number at 480 nm for the Resonator [16]. As Indicated, the Resonator Mirrors Were Located Either Inside or Outside of the Laser Gas Cell.

M	d (cm)	l/d	R_1 (m)	R_2 (m)	s (mm)	N_{eq}	Location
1.7	56	0.89	2.7	−1.6	21.0	138	internal
2.0	75	0.67	3.0	−1.5	17.5	106	external
2.5	90	0.56	3.0	−1.2	14.0	85	external
3.0	100	0.50	3.0	−1.0	11.5	71	external

The relevant coupled rate equations for the amplification process relating the photon flux q, gain G, and absorption loss L are as follows.

$$\frac{\partial q(x,t)}{\partial x} + \frac{1}{v_g}\frac{\partial q(x,t)}{\partial t} = G(x,t)\,q(x,t) - L(x,t)\,q(x,t) + \frac{N_C(t)}{\tau_{CA}}\frac{\Omega}{4\pi}\frac{\Delta\nu_I}{\Delta\nu_F} \tag{1}$$

$$\frac{\partial G(x,t)}{\partial t} = P_C(t)\,\sigma_{SE} - \frac{G(x,t)}{\tau_C} - G(x,t)\,\sigma_{SE}\,q_{eff}(x,t) \tag{2}$$

$$\frac{\partial L(x,t)}{\partial t} = P_{abs}(t)\,\sigma_{abs} - \frac{L(x,t)}{\tau_{abs}} - L(x,t)\,\sigma_{abs}\,q_{eff}(x,t) \tag{3}$$

where t is time and x is the position within the unfolded laser amplifier. v_g is the group velocity which is assumed to be constant and equal to the speed of light. N_C is the population of the upper XeF(C) state and τ_{CA}, τ_C, and τ_{abs} are the radiative lifetime of the XeF($C \rightarrow A$) transition, the effective lifetime of the XeF(C) state, and the effective absorber lifetime, respectively. Ω is the relevant solid angle for the emission of spontaneous photons that contribute to the output signal and $\Delta\nu_I$ and $\Delta\nu_F$ are the linewidth of the injection source and the bandwidth of the laser transition. σ_{SE} and σ_{abs} are, respectively, the cross section for stimulated emission of the XeF($C \rightarrow A$) transition and the estimated absorption cross section of the principal absorber species. q_{eff} is the effective photon flux for a given point in the resonator and is used for the treatment of gain and absorption saturation. It is different from the photon flux q due to the overlap of multiple beam passes through the gain medium as will be described in more detail in Section III-D.

The production terms for the XeF(C) excited states and the absorbers are denoted by $P_C(t)$ and $P_{abs}(t)$, respectively, and are calculated from the experimentally determined small signal gain and loss temporal profiles $G_0(t)$ and $L_0(t)$ using the unsaturated rate equations:

$$P_C(t) = \frac{1}{\sigma_{SE}}\left[\frac{dG_0(t)}{dt} + \frac{G_0(t)}{\tau_C}\right] \tag{4}$$

$$P_{abs}(t) = \frac{1}{\sigma_{abs}}\left[\frac{dL_0(t)}{dt} + \frac{L_0(t)}{\tau_{abs}}\right]. \tag{5}$$

B. Integration Technique

To solve the coupled differential equations (1)–(3) it is important to consider photons that originate from all points in the unfolded laser resonator. In the experiments presented here, quasi-CW injection was used: the injection pulse duration was significantly longer than the gain duration. It was not possible to simply eliminate the spatial dependence of the differential equations by introducing a local time variable since photons that entered the amplifier after the onset of gain (hence at negative local times) must also be considered in the amplification process. For this reason, an integration technique was adopted in which the temporal and spatial integrations were performed separately. For a given spatial point inside the unfolded cavity, the temporal gain and loss profiles were numerically integrated, using (2) and (3) and an integration step size of Δt, from time zero to some time after the termination of the gain pulse. A spatial step was than made to the next position in the amplifier such that the size of the step Δx corresponded to the photon transit distance during one temporal step $v_g \cdot \Delta t$. Therefore, in the computation, the numerical array representing the temporal profile of the photon flux was simply shifted forward by one element before making a spatial integration step using (1).

Given the above description, the injection signal was the temporal profile of the incident intensity at the first point in the resonator: the injection aperture. In the experiments that are presented here, the injection laser pulse was significantly longer than the XeF($C \rightarrow A$) gain pulse so a quasi-CW approximation was made by placing the same value in each element of the intensity array. Of course an injection pulse of a different shape or duration could be placed in this starting profile to simulate the propagation of a selected light pulse through the amplifier.

C. Resonator Magnification

The effect of the unstable resonator magnification is to present a distributed loss to the photon flux as the laser beam expands inside the laser cavity. In [7], this was modeled as a continuous exponential loss by the addition of the term $[-\ln(M)/d \cdot q(x, t)]$ to (1) where M is the resonator magnification and d is the spacing between the two mirrors. This approximation was shown to be very effective for the modeling of a cavity with a small magnification, resulting in a large number of round-trips through the laser resonator. A more general treatment, however, linearly expands the beam on every other pass through the cavity as depicted in Fig. 1. This was implemented by attenuating the laser flux by an appropriate factor before each spatial step. This factor was the ratio of the beam cross-sectional area before the step to that after the step and of course was equal to 1 during passes in which the beam was not expanding.

D. Overlapping Beam Passes

The most significant limitation of the one-dimensional rate equation analysis presented thus far is that it neglects the effects of multiple beam passes through the same gain volume and as a consequence, underestimates the saturation of gain and absorption. The ray tracing model depicted in Fig. 1 suggests that the laser flux passes twice through every point inside the active volume, except for the last portion of the final pass. The one-dimensional unfolded amplifier model can therefore overestimate the active laser volume and hence, extracted laser energy. The laser volume assumed by such a model exceeds the actual volume by only 33% for a large magnification three pass cavity, but approaches twice the actual volume for a small magnification cavity in which the non-overlapping volume of the final pass becomes negligible.

A simple approximation to treat this overlap is to set the saturation flux $q_{eff}(x, t)$ in (2) and (3) to twice the laser flux.

$$q_{eff}(x_i, t) = 2q(x_i, t). \tag{6}$$

That is, it is assumed that the overlapping beams passing through the same volume are of comparable intensity. This is a reasonable approximation since the change in intensity during one round-trip through the saturated amplifier is not large due to cavity magnification losses. However, a problem does arise when, during the amplification process, a temporally narrow laser pulse develops from the quasi-CW injection background. In this case the simple

factor of two correction overestimates the peak photon density since the pulse in the overlapping beam passes do not overlap in time. The peak intensities of the two beams can be offset in time by up to one round-trip through the resonator. This difficulty was overcome by temporally shifting the photon intensity profile for a given point inside the resonator to simulate the intensity contribution of an overlapping beam pass. Consider the point i located at position x_i on beam path A as shown in Fig. 2. For a spatial step Δx, there is overlap with beam paths B and C in the volumes represented as V_B and V_C. The effective photon flux array at this point, according the above scheme, is represented by

$$q_{\text{eff}}(x_i, t) = q(x_i, t) + \frac{1}{V_B + V_C}\left[V_B\, q(x_i, t_B) + V_C\, q(x_i, t_C)\right] \tag{7}$$

where

$$t_B = t + 2\frac{x_i}{v_g} \tag{8}$$

$$t_C = t - 2\frac{d - x_i}{v_g} \tag{9}$$

and d is the spacing between the resonator optics. In this manner the overlapping intensity profiles contributed by beam paths B and C are approximated by shifting the temporal photon flux array for point i on path A backward and forward, respectively, weighting it in each case by the corresponding size of the overlapping volume. This method effectively approximates the correct saturation behavior of gain and absorption in the laser medium while retaining the computational convenience of a one-dimensional calculation.

E. Unpumped Beam Path and Intracavity Losses

It is often the case that the cavity length d is greater than the length of the gain medium l and the ratio l/d has a significant impact on laser performance for the case of pulsed laser systems. It has been demonstrated that for a cavity of small magnification, when this ratio is sufficiently close to unity, it is reasonable to evenly distribute the gain along the entire cavity length by scaling the gain and loss terms in (1) by this factor [7]. Problems arise, however, as the ratio of the length of the active volume to the resonator length is decreased since this approximation neglects the nonradiative loss of excited state population during the transit time of the peak photon flux through the unpumped resonator volume. This also leads to an increased laser build-up time. In a more general treatment, the laser gain and loss are set to zero during integration steps outside of the laser medium. The only losses experienced in the unpumped regions are those that result from the beam magnification expansion. Losses due to resonator mirrors or intracavity optical elements such as the laser cell pressure windows are incorporated by attenuating the laser intensity temporal profile by the appropriate loss factor at the spatial points in the unfolded resonator where they occur.

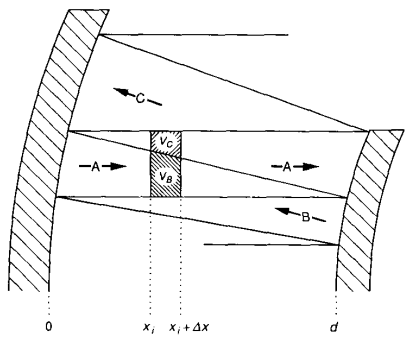

Fig. 2. An illustration of overlapping beam passes inside an unstable resonator of length d. For a spatial integration step Δx, the depicted volume in beam A overlaps with beam B in volume V_B and beam C in volume V_C.

F. Noninteger Round-Trips

For a given injection hole diameter, the unstable cavity magnification and the diameter of the output coupler can be chosen such that, on the next to the last round-trip, the laser beam outer diameter closely matches the diameter of the output coupler reflector (Fig. 1). In this case, the laser beam emerges from the cavity on the next round-trip as a single output ring. Otherwise, as shown in Fig. 3, one beam path through the cavity intersects the edge of the output coupler allowing a partial ring to be coupled out. The remaining light makes one more round-trip before escaping the resonator. This results in the output of two concentric laser beams temporally separated by the transit time for one cavity round-trip. This situation impacts the behavior of the observed laser output, resulting in a temporally broadened pulse, and should therefore be treated in the injection-control model. This was accomplished by recording the predicted photon flux temporal array at the output coupler just before the last trip through the resonator. The temporal profile of the laser output was then the weighted sum of this profile and the final intensity profile at the output coupler (Fig. 3), where the weighting factors were the respective areas of the two output rings. The result was the total output power profile which is then integrated to obtain the laser pulse energy.

G. Off-Axis Unstable Resonators

Up to this point, the model assumed a homogeneously distributed gain medium. For our experimental conditions, the attenuation of the transverse electron beam excitation in the laser gas, however, results in a gain gradient perpendicular to the optical axis. The gain coefficient varies over the total beam area by almost a factor of two, exhibiting a maximum value of 0.04 cm^{-1} at a position closest to the electron beam [14]. The dependence of the gain upon the distance from the optical axis is in good approximation a linear function. By using off-axis unsta-

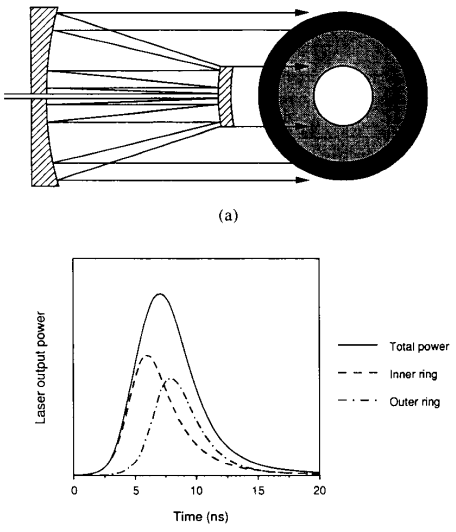

Fig. 3. (a) A noninteger number of cavity passes in an injection-controlled unstable resonator. The resulting output beam consists of two concentric rings, temporally separated by the transit time for one cavity round-trip. (b) The measured laser power profile is the sum of that of each beam component, resulting in the observation of a temporally broadened laser pulse.

ble resonators, it is possible to take advantage of this characteristic. In an unstable resonator, the beam area expands exponentially, making the initial passes through the cavity highly localized. Therefore, if the optical axis of the cavity is placed in a high gain region the total gain for an injected beam will be increased, leading to an increase in laser output in the unsaturated regime.

Despite the large gain variation for the maximum beam diameter of the final expansion path, for most of the amplification process the beam diameter is much smaller and consequently the gain variation in these passes is less important. In the final path the intensity is highest causing an early saturation of the gain and diminishing any gain inhomogenity effects. It is therefore a good approximation to average the gain over the transverse beam profile and use the averaged gain in the previously described one-dimensional treatment. This has the advantage of keeping the model simple and easily adaptable to personal computers.

IV. Experimental

A. Apparatus

The XeF($C \rightarrow A$) laser used in these experiments has a 0.48 L active gain volume that was 3.5 cm in diameter and 50 cm long [13], [14]. This volume was pumped by a 10 ns high current-density (~ 250 A/cm^2) electron beam with a peak voltage of ~ 650 kV and a peak current of ~ 85 kA which resulted in an average energy deposition of ~ 110 J/L in the laser gas [14]. The gas mixture for these experiments consisted of 8 T NF_3, 1 T F_2, 8 T Xe, and 1200 T Kr and was completed to 6.5 bar with an Ar buffer; a mixture developed to optimize XeF(C) production and to suppress transient absorption species [17].

The performance of the electron-beam pumped laser system was characterized on each shot by a set of simultaneously measured diagnostics. A pyroelectric energy meter, a vacuum photodiode, and an optical multichannel analyzer spectrometer recorded the laser output energy and temporal and spectral profiles, respectively. A calibrated second photodiode measured the dye laser injection pulseform and power. Voltage and current monitors in the electron-beam generator diode monitored the shot to shot system performance and provided timing reference signals for accurate laser pulse temporal delay measurements.

The injection source was an excimer pumped dye laser with a pulsewidth of 45 ns FWHM and a linewidth of ~ 0.005 nm. The output wavelength was tuned to 486.8 nm for these experiments; a point near the optimum gain for the XeF($C \rightarrow A$) system. To avoid the coupling of amplified light reflected from the output coupler of the amplifier backwards into the dye laser, the distance between the dye laser and the amplifier cell was set to 6 m for a round-trip transit time of 40 ns. The injection intensity was adjusted by placing neutral density filters at the injection laser output. With no attenuation, it was possible to deliver ~ 2 mJ through the unstable resonator injection hole corresponding to a peak intensity of ~ 3 MW/cm^2.

B. Laser Resonators

Two resonator optical configurations were employed for these studies. In the first, the cavity optics were located inside the laser gas cell. In this case, no additional optical elements were required between the laser mirrors and the length of the cavity was very closely matched to that of the pumped volume. The second configuration involved the placement of the reflectors outside the laser cell using antireflection coated windows tilted at 3°, allowing the cavity length to be freely adjusted. The external mounting configuration provided increased ease of alignment and removed the laser mirrors from direct contact with the potentially corrosive laser gas mixtures.

Experiments were performed using resonators of four different magnifications. For each magnification the diameter of the output coupler was chosen to maintain a laser beam diameter of 35 mm. The internally mounted resonator had a magnification of 1.7 with a cavity length of 56 cm and an output coupler diameter of 21.0 mm. Three external cavities were treated with magnifications of 2.0, 2.5, and 3.0 and with output coupler diameters of 17.5, 14.0, and 11.5 mm, respectively. In order to use the same input coupler for each of these, the cavity length was adjusted, maintaining a confocal mirror spacing. This resulted in cavity lengths of 75, 90, and 100 cm for the three external resonators. No attempt was made to optimize these lengths with respect to Fresnel number depen-

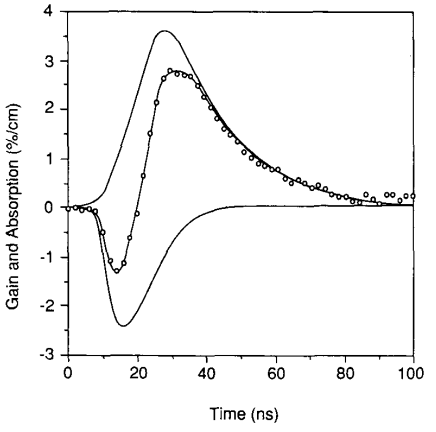

Fig. 4. Gain (top) and loss (bottom) temporal profiles used as model input for the experimental conditions described in the text. The center trace is the observed net gain profile and the open circles represent experimentally measured points. The shape of the gain profile is taken from a fluorescence measurement made through 5 cm of the gain volume and is scaled such that the resulting loss curve exhibits single component decay without crossing zero.

dent oscillations in cavity losses that have been reported for unstable resonators [6], [16]. An injection hole centered in the concave resonator mirror with a diameter of 1.5 mm was used in all cases. A summary of the unstable resonator parameters is presented in Table I.

C. Gain and Loss Measurements

The injection-control model required as input estimates for the small signal gain and loss temporal profiles. The most straightforward experimental observable, however, was the difference between the gain and loss $G(t) - L(t)$, i.e., the net gain $g(t)$. This measurement was made using a 250 ns flashlamp pumped dye laser probe directed along the optical axis. The dye laser was tuned to the same wavelength used in the injection-control studies (486.8 nm) and its peak intensity was attenuated to $\sim 50\ \mathrm{W/cm^2}$ to avoid saturation effects in the laser medium. For the gas mixture employed in these studies, the peak net gain was measured to be $2.6\ \mathrm{cm^{-1}}$ as illustrated in Fig. 4.

The temporal shape of the gain curve in the absence of absorption could be inferred from the fluorescence output of the laser cell without resonator optics installed. In order to minimize distortion by amplified spontaneous emission, an optical baffle was inserted into the cell to reduce the length of the fluorescence volume to 5 cm. To generate $G(t)$, the measured fluorescence output curve was scaled so that the absorption curve, given by $L(t) = G(t) - g(t)$, exhibited single exponential decay without crossing zero (Fig. 4). This setting was supported by almost exact agreement with the predictions of kinetic modeling [17] for these experimental conditions. The XeF(C) state and absorber production rate profiles were then calculated from $G(t)$ and $L(t)$ using (4) and (5).

V. Modeling of Experimental Measurements

For the laser experiments at 486.8 nm, the cross section for stimulated emission σ_{SE} was set to $9 \times 10^{-18}\ \mathrm{cm^2}$ [18]. The broad-band absorptions in the electron-beam excited laser mixture are predominantly the result of the photoionization of highly excited rare gas species [17] and therefore a cross section for absorption σ_{abs} of $2 \times 10^{-17}\ \mathrm{cm^2}$ was chosen as representative of these processes. An earlier version of the model [7] used a smaller absorption cross-section σ_{abs} of $3 \times 10^{-18}\ \mathrm{cm^2}$, only one third of the gain cross section, reflecting the initial assumption that molecular ion photodissociation is the main source of broad-band absorption. The larger absorption cross section used in the present model leads to stronger saturation of absorbers at high laser fluences, which significantly affects the saturation behavior of the amplifier. For the XeF($C \rightarrow A$) system, saturation of absorbers results in a calculated output energy increase of almost a factor of two. Furthermore, at a larger degree of absorber saturation the model predictions become more sensitive to the absolute gain and absorption coefficients rather than just to the net gain. The more comprehensive geometrical treatment of saturation processes in the present version enables the use of a higher value for the absorption cross section which is in better agreement with predictions by a kinetic model of the XeF($C \rightarrow A$) gain medium [17].

The effective lifetime of the XeF(C) excited state τ_C and that of the absorber species τ_{abs} were set to 15 and 6 ns, respectively, and a measured value of 100 ns was used for the lifetime for spontaneous emission τ_{CA} [19]. The ratio $\Delta\nu_I/\Delta\nu_F$ was set to 1×10^{-4}, corresponding to an injection linewidth $\Delta\nu_I$ of 0.005 nm and a XeF($C \rightarrow A$) transition bandwidth $\Delta\nu_F$ of 50 nm. The solid angle for spontaneous emission Ω was defined by the fractional solid angle from the midpoint of the cavity to the 1.5 mm injection hole. The spontaneous emission term [right-hand side of (1)] did not significantly impact the predicted laser performance for the injection-controlled XeF($C \rightarrow A$) laser due to its low rate of spontaneous emission. It was therefore found that the calculations were fairly insensitive to the exact settings of τ_{CA}, $\Delta\nu_I$, $\Delta\nu_F$, and Ω.

For the external cavity simulations, a measured loss of 1.5% was used for each of the antireflection coated laser cavity windows. It was observed that the transmission of the windows quickly degraded to ~98.5%, presumably due to interaction with the laser gas, but remained stable at this value for the duration of the experiments. The window losses result in a calculated decrease in output energy on the order of 10% depending on experimental conditions. No losses were assumed for the laser resonator optical coatings since the measured reflectivity was better than 99.8%.

VI. Results and Discussion

The experimentally measured output energies of the laser system for the four resonator configurations as a function of injection intensities between $3\ \mathrm{kW/cm^2}$ and

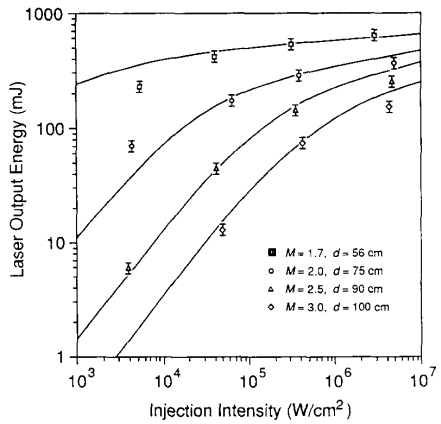

Fig. 5. Output energy versus injection intensity for the four resonator configurations investigated. The symbols represent experimental measurements and the solid curves are the results of the model simulations. Squares: $M = 1.7$ internally mounted 56 cm resonator, circles: $M = 2.0$ externally mounted 75 cm, triangles: $M = 2.5$ externally mounted 90 cm, and diamonds: $M = 3.0$ externally mounted 100 cm.

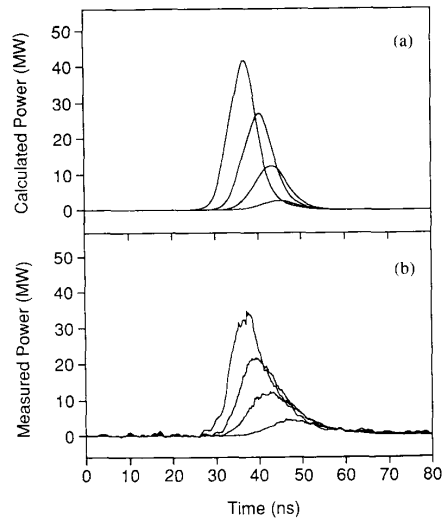

Fig. 6. A comparison of calculated (a) and experimentally observed (b) laser output temporal profiles for the $M = 2.0$ externally mounted unstable resonator with a mirror spacing of 75 cm. In each case, the traces from the top to bottom correspond to injection intensities of 3000, 300, 30, and 3 kW/cm^2.

3 MW/cm^2 are presented as points on the graph in Fig. 5. The error bars are given by an uncertainty in the absolute calibration of the energy meter of $\pm 10\%$. Complete injection control of the laser output for all of the reported points was confirmed by simultaneous spectral measurements.

The solid lines in Fig. 5 are the predicted output energies that result from the modeling calculation presented here. Good agreement exists between the experimental measurements and the numerical results of the simulation, both in terms of the qualitative trends of the laser saturation behavior and the prediction of absolute energy levels. For low injection intensities, the shortened transit distance through the large magnification resonators does not allow the injected intensity to approach the saturation level and the laser output energy is reduced. This situation can be overcome, however, by providing a more intense starting field using increased injection signal as illustrated by the convergence of the output energy curves at the highest injection intensities. This effect is partially masked in these experiments due to the decreased performance resulting from the larger mirror spacing and intracavity laser window used with the higher magnification resonators. The increase in performance at greater injection intensities is of particular significance for applications that benefit from the improved beam quality provided by larger cavity magnifications [20]. On the other hand, the choice of a magnification near the predicted energy extraction optimum results in very efficient injection control of the laser amplifier at low injection intensities. For the magnification 1.7 resonator, the laser output drops by less than a factor of three when the injection intensity is reduced by three orders of magnitude from ~ 3 MW/cm^2 to ~ 3 kW/cm^2.

Good agreement between calculated and experimentally measured data also exists for the temporal laser output profiles. Fig. 6 shows a comparison of the predicted and experimentally observed profiles as a function of injection intensity for the resonator with a magnification of 2 and a cavity length of 75 cm. From the highest peak to the lowest, the curves correspond to injection intensities of 3000, 300, 30, and 3 kW/cm^2. As shown, the predicted pulsewidths, peak intensities, and pulse delays are in excellent agreement with the experimental measurements. Comparable consistency between the measurements and the numerical predictions also exists for the other resonator configurations. It is important to note that the predicted outputs are not the result of a numerical fitting procedure but are produced by a model with no adjustable input parameters.

Fig. 7 compares measured and calculated energy outputs of off-axis unstable resonators for different resonator axis positions (see Section III-G). The resonators were mounted externally to the excimer gas cell and had a magnification of $M = 2$. Square resonators were chosen to better match the active gain area and to simplify gain averaging calculations. The output energy is higher for configurations with the optical axis closer to the e-beam, reflecting the increased total gain in this case. For higher injection intensities the output energies of the different resonators converge on a common constant energy level. This is expected, since for injection intensities sufficiently high to saturate the gain the output energy only depends on the stored energy in the cavity. The use of an off-axis resonator results in lower input intensity requirements and a higher locking efficiency, even though the maximum output remains unaffected. The saturation behavior and energy for different resonator configurations are predicted

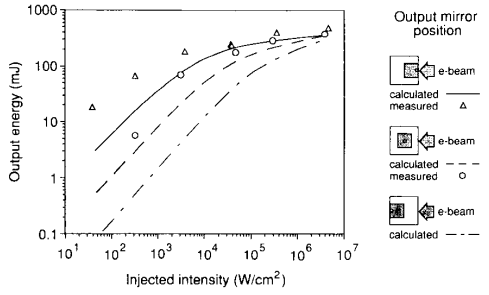

Fig. 7. Dependence of XeF($C \rightarrow A$) laser output energy on the injected intensity for different resonator configurations. Experimental and modeling results are compared. The square, external resonator has a magnification of $M = 2$ and a cavity length of 75 cm. Two intracavity windows each contribute losses of 1.5%. The legend icons depict the resonator configuration relative to the transverse electron beam excitation. The outer square gives the full beam area, the shaded smaller square represents the output coupler, and the small circle indicates the position of the optical axis.

correctly. For low injection intensities the model predicts higher output energies than measured, but shows the correct qualitative trends.

In conclusion, the application of a simple one-dimensional analytical model has been successfully demonstrated for the design of a scaled XeF($C \rightarrow A$) injection-controlled laser system. The described enhancements to the original model have resulted in the accurate simulation of the excimer laser output for a variety of unstable resonator magnifications, mirror spacings, and intracavity optical losses. Parts of this model have also been used to design unstable resonators for subpicosecond pulse energy extraction from a XeF($C \rightarrow A$) excimer laser amplifier [21]. As such, the analytical model can be used as a very effective predictive tool for the investigation of injection-controlled pulsed laser performance over a broad range of design parameters.

REFERENCES

[1] H. Tashiro, T. Shimada, K. Toyoda, and S. Namba, "Studies on injection locking of a TEA-CO_2 laser for stable high-power operation," *IEEE J. Quantum Electron.*, vol. QE-20, pp. 159-165, 1984.

[2] I. Petitbon, P. Gallion, G. Debarge, and C. Chabran, "Locking bandwidth and relaxation oscillations of an injection-locked semiconductor laser," *IEEE J. Quantum Electron.*, vol. 24, pp. 148-154, 1988.

[3] Y. K. Park, G. Giuliani, and R. L. Byer, "Single axial mode operation of a Q-switched Nd:YAG oscillator by injection seeding," *IEEE J. Quantum Electron.*, vol. QE-20, pp. 117-125, 1984.

[4] P. Flamant and G. Mégie, "Frequency locking by injection in dye lasers: Analysis of the CW and delta pulse regimes," *IEEE J. Quantum Electron.*, vol. QE-16, pp. 653-660, 1980.

[5] C. B. Dane, S. Yamaguchi, T. Hofmann, R. Sauerbrey, W. L. Wilson, and F. K. Tittel, "Spectral characteristics of an injection-controlled XeF($C \rightarrow A$) excimer laser," *Appl. Phys. Lett.*, vol. 56, pp. 2604-2606, 1990.

[6] I. J. Bigio and M. Slatkine, "Injection-locking unstable resonator excimer lasers," *IEEE J. Quantum Electron.*, vol. QE-19, pp. 1426-1436, 1983; see also *Opt. Lett.*, vol. 7, pp. 19-21, 1982.

[7] N. Hamada, R. Sauerbrey, and F. K. Tittel, "Analytical model for injection-controlled excimer laser amplifiers," *IEEE J. Quantum Electron.*, vol. 24, pp. 2458-2466, 1988.

[8] A. A. Isaev, M. A. Kazaryan, G. G. Petrash, S. G. Rautian, and A. M. Shalagin, "Shaping of the output beam in a pulsed gas laser with an unstable resonator," *Sov. J. Quantum Electron.*, vol. 7, pp. 746-752, 1977.

[9] Y. A. Anańev, "Establishment of oscillations in unstable resonators," *Sov. J. Quantum Electron.*, vol. 5, pp. 615-617, 1975.

[10] A. Icsevgi and W. E. Lamb, Jr., "Propagation of light pulses in a laser amplifier," *Phys. Rev.*, vol. 185, pp. 517-545, 1969.

[11] T. F. Johnson, Jr., L. J. Palumbo, and A. M. Hunter, II, "Kinetics simulation of high-power gas lasers," *IEEE J. Quantum Electron.*, vol. QE-15, pp. 289-301, 1979.

[12] N. Hamada, R. Sauerbrey, W. L. Wilson, F. K. Tittel, and W. L. Nighan, "Performance characteristics of an injection-controlled electron-beam pumped XeF($C \rightarrow A$) laser system," *IEEE J. Quantum Electron.*, vol. 24, pp. 1571-1578, 1988.

[13] G. J. Hirst, C. B. Dane, W. L. Wilson, R. Sauerbrey, F. K. Tittel, and W. L. Nighan, "Scaling of an injection-controlled XeF($C \rightarrow A$) laser pumped by a repetitively pulsed, high current density electron beam," *Appl. Phys. Lett.*, vol. 54, pp. 1851-1853, 1989.

[14] C. B. Dane, G. J. Hirst, S. Yamaguchi, T. Hofmann, W. L. Wilson, R. Sauerbrey, F. K. Tittel, W. L. Nighan, and M. C. Fowler, "Scaling characteristics of the XeF($C \rightarrow A$) excimer laser," *IEEE J. Quantum Electron.*, vol. 26, pp. 1559-1568, 1990.

[15] S. Yamaguchi, T. Hofmann, C. B. Dane, R. Sauerbrey, W. L. Wilson, and F. K. Tittel, "Repetitively pulsed operation of an injection controlled high power XeF($C \rightarrow A$) excimer laser," *IEEE J. Quantum Electron.*, vol. 27, pp. 259-262, 1991.

[16] A. E. Siegman, "Unstable optical resonators," *Appl. Opt.*, vol. 13, pp. 353-367, 1974.

[17] W. L. Nighan and M. C. Fowler, "Kinetic processes in electron beam-excited XeF($C \rightarrow A$) laser media," *IEEE J. Quantum Electron.*, vol. 25, pp. 791-802, 1989.

[18] W. K. Bischel, D. J. Eckstrom, H. C. Walker, Jr., and R. A. Tilton, "Photolytically pumped XeF($C \rightarrow A$) laser studies," *J. Appl. Phys.*, vol. 52, pp. 4429-4434, 1981.

[19] R. Sauerbrey, W. Walter, F. K. Tittel, and W. L. Wilson, "Kinetic processes of electron beam generated XeF* and Xe_2F* excimers," *J. Chem. Phys.*, vol. 78, pp. 735-747, 1983.

[20] J. M. Eggleston, "Theory of output beam divergence in pulsed unstable resonators," *IEEE J. Quantum Electron.*, vol. 24, pp. 1302-1311, 1988.

[21] T. Hofmann, T. E. Sharp, P. J. Wisoff, W. L. Wilson, F. K. Tittel, and G. Szabó, "Characterization of an ultrahigh peak power XeF($C \rightarrow A$) excimer laser system," *IEEE J. Quantum Electron.*, to be published.

C. Brent Dane, for a photograph and biography, see p. 262 of the February 1991 issue of this JOURNAL.

Thomas Hofmann, for a photograph and biography, see p. 262 of the February 1991 issue of this JOURNAL.

Roland Sauerbrey (M'85-SM'90), for a photograph and biography, see p. 99 of the January 1991 issue of this JOURNAL.

Frank K. Tittel (SM'72-F'86), for a photograph and biography, see p. 100 of the January 1991 issue of this JOURNAL.